JOURNAL OF OPTOELECTRONICS AND ADVANCED MATERIALS Vol. 8, No. 6, December 2006, p. 1969 - 1978

Reduction of defects by network self-organizations in non-crystalline dielectrics and semiconductors: *a tribute to Professor Radu Grigorovici on the occasion of his 95th birthday*

G. LUCOVSKY, J. C. PHILLIPS[a]

Department of Physics, NC State University, Raleigh, NC 27695-8202, USA

[a]Department of Physics, Rutgers University, Piscataway, NJ 08854, USA

This review paper has been penned to celebrate the 95th birthday of Professor Radu Grigorovici. He is truly on of the giants in the field, providing significant seminal insights into the bonding and electronic structure of non-crystalline solids. These have proved to be the foundation for the development of many of the device applications addressed in this paper, and equally important as a source of inspiration to those of us who have developed an increased understanding of this technologically important class of solids. Studies of binary chalcogenide alloys have established that the onset of network rigidity is generally *delayed* by a network self-organization resulting in an intermediate phase with significant deviations from mean-field chemical bonding. In Ge_xSe_{1-x}, the onset of local chemical bonding rigidity occurs for a mean-field coordination, $r_c = 2.4$ at $x = 0.2$, but percolation of stress resulting in network rigidity is delayed until $r_c = 2.52$. This paper demonstrates that low levels of electrically active defects in i) gate dielectrics for (a) thin film transistors (TFTs) in liquid crystal displays (LCDs), and (b) aggressively-scaled metal-oxide-semiconductor field effect transistors (MOSFETs), The driving for force for this self-organizations is the suppression of macroscopic strain that presents an energy-favorable trade-off between changes in configurational entropy and reductions in macroscopic strain energy.

(Received October 11, 2006; accepted November 2, 2006)

Keywords: Thin film dielectrics, Thin film amorphous semiconductors, a-Si thin film transistors, c-Si field effect transistors, photovoltaic devices, Strain relieving network self-organizations, Intermediate phases, Chemically-order bonding, Hydrogenated silicon nitrides, Zr Si oxynitrides, Hydrogenated amorphous silicon

1. Introduction

Two different aspects of band alignment and bonding in gate dielectrics are required to optimize field effect transistor (FET) devices. These include (a) thin film transistors (TFTs) with hydrogenated amorphous/non-crystalline/amorphous silicon, a-Si:H, transport channels, and (b) advanced and aggressively-scaled FETs with crystalline silicon, c-Si, transport channels. The first optimization identifies the surface recombination and/or band alignments at semiconductor-dielectric interfaces. The second, and more challenging aspect has been a demonstration that strain-reducing, network self-organizations, and the formation of strain-free intermediate interface and bulk phases, are crucial for the applications cited above. The same considerations apply to a-Si(H) alloys.

This research approach is reflected in the organization of the article. Section 2 presents research results that describe properties of thin film a-SiO_2 and a-$Si_xN_yH_z$ deposited directly onto a-Si:H substrates at 300 °C. This processing temperature establishes the H-atom concentrations in a-Si:H channels, and doped a-Si source and drain contacts required for optimization of device performance and reliability. The dielectric/a-Si interfaces have been studied by analysis of photo- and dark-currents in sandwich and surface cell geometries [1,2]. These results have been correlated with threshold voltages for electrical switching in TFTs. The optimum dielectric for a-SiH TFTs has been demonstrated to be a heavily hydrogenated a-$Si_xN_yH_z$ alloy with approximately 28-30% Si, 42-40% N and 29-31% H. In contrast, stoichiometric a-SiO_2 is the optimum gate dielectric for c-Si:H TFT devices [3]. Section 3 addresses FETs for aggressively-scaled Si complementary metal oxide semiconductor (CMOS) logic and memory circuits. These require a gate dielectric with an equivalent oxide thickness (EOT) <1.5 nm, and ultimately <1.0 nm, in order to maintain the high drive-currents required for ultra-fast switching times, << 1 ns. These CMOS device require high-k alternative dielectrics other than SiO_2 to reduce tunneling leakage to levels where it does not degrade FET performance and reliability [4]. Recent studies have demonstrated that a-Zr (and Hf) Si oxynitride alloys provide a viable engineering solution for EOTs extending to about 0.7-0.8 nm [5]. Section 4 presents a discussion of experimental results that indicate qualitative and quantitative similarities in the chemical bonding of the a-SiN:H and a-Zr Si oxynitride alloy compositions that have been optimized for device applications. These properties are indicative of network

self-organizations that create intermediate phases with low defect/defect precursor concentrations similar to those addressed at length for chalcogenide alloys by Boolchand and co-workers [6].

The dielectric thin films of this article have been prepared by remote plasma enhanced chemical vapor deposition (RPECVD) at 300 °C; details of film deposition processes and analytical techniques used to define their chemical composition are discussed in Refs. 3, 7 and 8. In the a-$Si_xN_yH_z$ alloys for TFT applications, self-organization occurs during deposition [9]. In the a-$(SiO_2)_x(Si_3N_4)_y(ZrO_2)_{1-x-y}$ alloys for logic and memory cell FETs, these chemical network self-organizations occur during high-temperature anneals at temperatures of approximately 900 °C [10].

Finally, Section 4 focuses on thin films of hydrogenated a-Si(H) and Section 5 summarizes the main ideas of the paper, and the universality of these self-organizations in non-crystalline alloy systems with disparate bonding chemistries.

2. Gate dielectrics for TFTs

Dark- and photo-conductivity (PC) studies of a-Si:H interfaces with a-SiO_2 dielectrics have been made using a surface cell geometry [1]. By studying dark-conductivity as a function of the a-Si:H thickness an up-ward surface band-bending of ~0.2 eV was found at the a-Si:H/a-SiO_2 interface. This was subsequently correlated with a significant drop in photoconductivity (PC) for incident photon wavelengths < ~500 nm, and additionally and more importantly with relatively high threshold voltages, >3 V, for current drive turn-on in TFT devices with a-SiO_2 gate dielectrics [3]. These results for a-Si:H/a-SiO_2 interfaces were confirmed in a second series of experiments using sandwich cell structures [2].

These experiments indicated that a-Si:H surfaces exposed to air oxidize sufficiently to result in decreases in PC at short-wavelengths of 400-450 nm for both a-SiO_2 as well as a-SiN:H dielectrics [2]. In contrast, the PC response was relatively flat as a function of wavelength for a-SiN:H interfaces with a-Si:H formed by deposition of a-Si:H on a-SiN:H. The PC response for these a-Si:H/a-SiN:H interfaces correlated directly with reductions in TFT threshold voltages to < 2 eV [3].

For plasma-deposited a-SiN:H alloys, the source gas ratio, R= NH_3/SiH_4 determines the relative concentrations of Si, N, and H in the deposited thin films. R = 2-7 gives sub-nitride films with Si-Si bonding for N:Si ratios less than 1.3 and H bonded predominantly in Si-H groups [3], whereas R = 12-15 gives films with N:Si ratios greater than 1.6 and no detectable Si-Si bonding with H is bonded initially in Si-NH_2, and eventually in SiH_2 groups as well [3]. The bonding arrangements of H in the a-SiN:H films were determined from infra-red absorption measurements; Si-H groups have a bond stretching vibration at ~2100-2150 cm^{-1} in the alloys deposited with R = 2-7, and the SiN-H_2 groups in alloys deposited with R > 12 have a significantly higher stretching frequency, ~3300 cm^{-1}, as well as additional bending and rocking modes in the spectral range between about 1100 and 1300 cm^{-1} [3]. There is a narrow range of source gas ratios, R=10±0.5, with N/Si ratios of ~1.5±0.05 in which the H atom incorporation is predominantly in SiN-H groups, and it is in this narrow range of compositions that the current drive, and electron channel mobilities display their highest values [3] (see Fig. 1(a)).

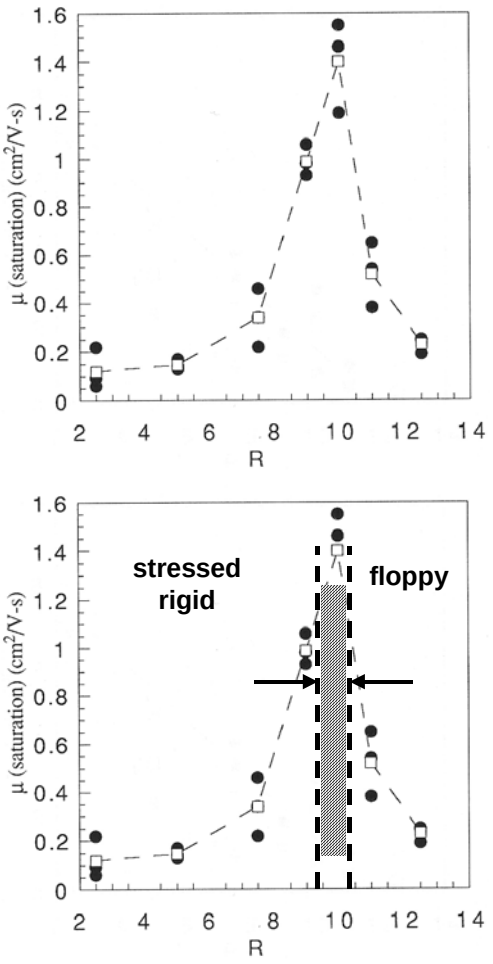

Fig. 1. (a) Effective channel mobility, , for a-Si:H TFTs with hydrogenated silicon nitride dielectrics as a function of R, the NH_3 to SiH_4 flow rate ratio of the process gases used in plasma-assisted deposition. (b) The same plot as in (a), but including a hatched region to indicate the compositional range corresponding to an intermediate phase.

The narrow regime of alloys compositions defines an intermediate phase between a floppy regime for R >11, and stressed-rigid regime for R < 9 [6, and references therein]. Mean-field values of the number of bonds/atom, r_c (also sometimes designated as N_{av}) of the number of bonds/atom, and n_c (also sometimes designated as C_{av}) confirm the *special character* of the bonding in this narrow composition range; e.g., an alloy composition with Si:N:H equal to ~0.30:0:40:0.30, with an uncertainty of ±0.02, yields r_c = 2.7±0.05, and n_c = 3.05±0.1. r_c is determined by the number of bonds per atom, m: 4 for Si, 3 for N and 1 for H, and is simply given by 4x0.30 +

3×0.40 + 1×0.30 or 2.70±0.05. n_c is determined by the number of bond-stretching and bond-bending valence force constraints per-atom and the chemical bonding model for this composition. Every Si-atom has 4 N-atom neighbors; the number of bond-stretching constraints per Si-atom is 0.5 m = 2, and the number of bond-bending constraints in 2m - 3 = 5. This gives 0.6 bond-stretching constraints and 1.5 bond-bending constraints, so that the Si-atom contribution, n_c(Si) = 2.1. Infrared spectra indicate predominantly N-H bonding arrangements at this composition, so that 75% of the N-atoms, or equivalently 0.3 N-H groups are functionally equivalent to bridging O-atoms in Si-O-Si arrangements in SiO_2, and incorporated in bridging arrangements as well. These contribute 1 bond-stretching and 1 bond-bending constraint or 0.6 constraints. The remaining 25% of the N atoms are also in planar arrangements and contribute 1.5 stretching constraints/N-atoms and m - 1 = 2 bond-bending constraints/N-atom [9], or an additional 0.35 constraints. n_c then equals 2.1 + 0.6 + 0.35 or 3.05±0.1 constraints/atom. This is a value of n_c that corresponds to an ideal stress-free network. For concentrations of NH_3 in the source gas mixture > 10, the gate dielectric is N-rich, and is in the floppy regime: for R ~12-13, r_c ~ 2.1, and n_c ~ 2. For concentrations of NH_3 in the source gas mixture less than 9, the gate dielectric is Si-rich, and is in the stressed-rigid regime: for R ~7-9, r_c ~ 3.2, and n_c > 4.

Based on the results presented in Ref. 3, the range of r_c values in the highlighted region of Fig. 2(b) is ~±0.15±0.05, and is approximately the same compositional range as identified for intermediate phases in chalcogenide binary alloys such as Ge_xSe_{1-x} [6,11]. This regime of alloy compositions is characterized by a network self-organization that minimizes the percolation of bond strain, and additionally *effectively eliminates* defects and defect precursors.

The minimization of bonding defects in the intermediate phase compositions in the a-SiN:H dielectrics has been *detected electrically* in the TFTs by the variation of the drive current and the channel mobility in the TFTs. The TFT channel mobility, μ, varies with the source gas ratio R [3], and therefore with the ratio of the Si:N:H alloy atom compositions; e.g., μ < 0.5 $cm^2V^{-1}cm^{-1}$ for R <8 and R >11, but μ >1.2 $cm^2V^{-1}cm^{-1}$ for R in a narrow range between ~9.5 and 11 (see Figs. 1(b)and 2(b)). The maximum value of μ is 1.5 $cm^2V^{-1}cm^{-1}$ at ~$Si_{0.3}N_{0.4}H_{0.3}$. As noted above, for this narrow range of compositions the average number of bonds/atom, r_c ~2.7±0.05, and the average number of bonding constraints/atom, n_c =3.05±0.1. These values of r_c and n_c are *indicators* of a network self-organization that suppresses percolation of network rigidity, thereby reducing intrinsic bonding defects that can trap channel electrons and lower the TFT drive current [6,11]. Since defect precursors are also reduced in the intermediate phase, defect generation during TFT operation is also reduced thereby increasing device reliability as reflected in the long term stability of flat panel displays in note book computers, and the like. Finally the plot in Fig. 2(b) represents the first electrical detection of an intermediate self-organized non-crystalline alloy phase.

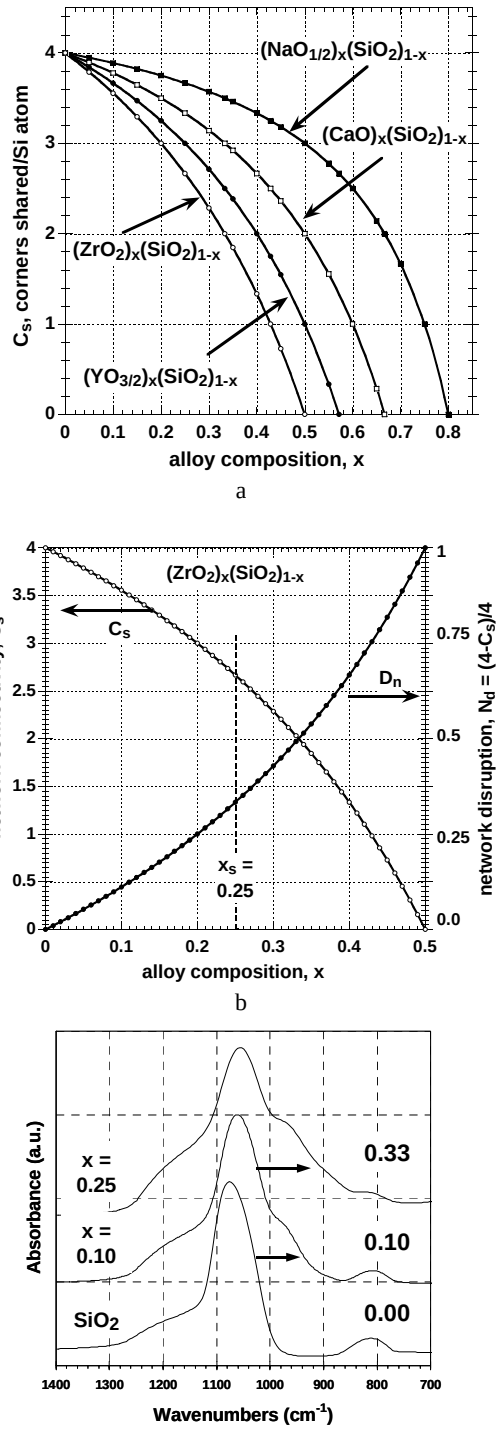

Fig. 2. (a) C_s, the number of shared corners/tetrahedrally-bonded Si-atom, versus x for Na silicates and Zr silicates. (b) D_n, the fraction of network disruption, and C_s are compared for Zr silicates. (c) Infrared absorption spectra in the spectral range of the Si-O asymmetric bond-stretching vibration for SiO2 and two different Zr silicate alloys with different ZrO_2 content, x=0.1 and x =0.5. The plot also includes values of D_n, the fraction of network disruption, 0.0 for SiO_2, and 0.1 and 0.3, for x=0.1,and 0.25, respectively.

3. Gate dielectrics for advanced c-Si FETs

The search for a high-k dielectric (k~20 or more) utilizing an inherently nano-crystalline transition metal (TM) or trivalent lanthanide rare earth atom (RE) elemental or complex oxides is rapidly coming to a close [5]. These dielectrics have been demonstrated to have two types of intrinsic bonding defects associated with O-atom vacancies [12,13], that render operation in CMOS devices, e.g., inverter configurations required for logic and memory applications, virtually impossible. These defects include hole and electron traps at negatively-charged and neutral O-atom vacancies at the metallurgical interfaces between the high-k dielectrics and ultra-thin SiO_2 and nitrided SiO_2 interfacial layers (ILs) [14,15], as well as in the bulk high-k dielectric films.

Studies of a-Zr silicate alloys with smaller values of k (~7 to 15) have demonstrated an inherent instability with respect to chemical phase separation (CPS) into a-SiO_2, and nanocrystalline Zr oxide when subjected to processing temperatures required for process integration, ~900 °C [8-10]. Similar instabilities are also inherent to a-Hf silicate alloys. In order to understand the way that CPS in a-Zr(Hf) silicates can be suppressed by including Si_3N_4 as a third alloy constituent, studies addressing the inherent instability in a-Zr silicates are summarized. These instabilities derive primarily from network disruption or break-up produced by the incorporation of ionic metal oxides, e.g., ZrO_2 and HfO_2 in the a-SiO_2 host network.

The *network disruption* produced by incorporation of ZrO_2 into SiO_2, has been addressed by considering the degree of *connectedness* of the host SiO_2 continuous random network (CRN) in the context of corner-connected $SiO_{4/2}$ tetrahedra, i.e., four-fold coordinated Si-atoms and with four two-fold coordinated O-neighbors. Network connectivity in a-$(ZrO_2)_x(SiO_2)_{1-x}$ thin film alloys is quantified by determining the number of *shared* corners/tetrahedrally-bonded Si-atom, defined here as C_s, as a function of function of the ZrO_2 content, x [8]. Each Zr atom introduced into a-SiO_2 by alloying with ZrO_2 introduces a concentration of terminal O-atoms equal to its formal chemical valence of four (4).

C_s is equal to two times the number of O atoms minus the number of terminal O-atoms, equal to the formal valence of metal of the metal oxide, divided by the total number of Si atoms [8]. As examples, for $(Na_2O)_x(SiO_2)_{1-x}$ alloys, $C_s = [2(2-2x)/(1-x)]$, and for $(ZrO_2)_x(SiO_2)_{1-x}$ alloys, $C_s = [2(2-4x)/(1-x)]$. Fig. 2(a) compares the *mean-field* or *statistically averaged* C_s as a function of the metal atom valence for monovalent, divalent, trivalent and tetravalent metal oxide silicate alloys. For purposes of comparison, the metal oxide compositions are expressed in terms a one atom representation: $NaO_{1/2}$, CaO, $YO_{3/2}$ and ZrO_2. This approach identifies a monotonic relationship between network disruption at a given ionic metal oxide composition, x, and the chemical valence of the metal atom as indicated in Fig. 2(a).

Referring to the plots in Fig. 2(a), the completely connected or ideal SiO_2 network is characterized by $C_s = 4$, and complete network disruption or break-up occurs when $C_s = 0$, i.e., when the positively charged metal ions are completely compensated by discrete $SiO4^{4-}$ molecular ions. $C_s = 3$, 2 and 1 indicate progressively increased network disruption; e.g., for $C_s = 1$ the metal ions are compensated by discrete $Si_2O_7^{6-}$ molecular ions, while for $C_s = 2$ and 3 there is proportionally more interconnection between the tetrahedral building blocks. For values of x greater than the value at which $C_s = 0$, the network is *inverted*, and the metal atom concentration is greater than the Si atom concentration.

Fig. 2(b) expands the scaling relationships for Zr silicates in terms of *network disruption or break-up, D_n,* and includes a comparison with the *corner-connectivity, C_s* plot. The fraction of network disruption D_n is given by $(4-C_s)/4$, and is plotted as a function of x for the a-Zr silicates. Fig. 2(c) displays an expanded plot of the Si-O bond-stretching infra-red response for SiO_2 and for two as-deposited low ZrO_2 content Zr silicate alloys with x = 0.10 and x = 0.25 [8]. The spectral feature centered at approximately 1060 cm^{-1} in these films is an asymmetric SiO_2 network mode. In this mode the atomic motions of the two-fold coordinated O-atoms are in a direction parallel to a line joining their two Si-atom neighbors, which in turn move in opposite directions. The high wavenumber shoulder at ~1160 cm^{-1} is a second Si-O stretching mode also associated with O-atom displacements, and induced by network disorder. The shoulder on the low wave number side of the peak at ~950 cm^{-1} is qualitatively different, and is assigned to terminal Si-O bonding groups, and therefore directly related to network disruption. The increase in the relative strength of this feature in Fig. 2(c) between SiO_2, and two silicate alloys with x~0.1 and 0.25 is consistent with the network disruption plot in Fig. 2(b) as applied to these as-deposited films. As has been demonstrated in Refs. 15 and 16, these a-Zr silicate thin films, as well all other a-Zr silicate thin films with compositions up to at least 75% ZrO_2 chemically phase separate (CPS) after annealing to 900 °C. This consistent with a liquid immiscibility dome or *spinoidal* centered at about 30% ZrO_2 in the equilibrium phase diagram for the ZrO_2-SiO_2 binary system [17].

One aspect of network modification for Zr silicate alloys is defined by increases in the coordination the O-atoms of the CRN SiO_2 host that are required to accommodate the bonding coordination of the Zr metal atoms that exceed the 8-N rule. The bonding coordination of Zr, C_{Zr}, in crystalline Zr silicate, $ZrSiO_4$ is equal to eight (8) for $ZrSiO_4$. In the Zr silicate alloys, it is an increasing linear function of the Zr content for values of x between 0.0 and 0.5; i.e., $C_{Zr} = 4+2x$. It is equal to 4 for very low content alloys, < 0.01, and reaches a mean-field value of eight (8) at the x = 0.5, or the $ZrSiO_4$ compound composition. It remains at eight for inverted silicates between x = 0.5 and 1.0.

The number of terminal $Si\text{-}O^{1-}$ bonding arrangements created by the addition of each ZrO_2 group is four (4), and this results in the formation of four ionic bonds between Zr and these terminal $Si\text{-}O^{1-}$ bonding arrangements. As x increases, and the network disruption increases and mean-field average in the number of ionic bonds increases as

well. The increase is linear as a function of x, and occurs because more than one Zr atom becomes a nearest neighbor to a given $Si\text{-}O^{1-}$ bonding group. At a concentration of x = 0.5, the mean-field average coordination of O-atom neighbors is three just as it is in the $ZrSiO_4$ crystal phase. In the completely disrupted network, two of these O-atoms make ionic bonds to Zr^{4+} ions, and the third O-atom bond is to the Si atom of the SiO_4^{4-} molecular ions. The difference between the saturated/preferred bonding coordination of eight for Zr, and reduced coordination of Zr for ZrO_2 concentrations between 0.0 and 0.5, results in an additional network *modification* in which non-bonding pairs on two-fold coordinated network O-atoms with a 2p π symmetry become oriented towards the Zr^{4+} ions, and thereby contribute to an electrostatic field at the Zr ion sites. This polarization contribution to the local ion field persists up to a concentration of about x = 0.25 to 0.3 or a 25% to 30% molecular fraction of ZrO_2. This is concentration at which the mean-field network disruption has increased to a point where the majority of the two-fold coordinated Si atoms are in molecular ion arrangements, rather than included as connected Si-O-Si groups of an ideal CRN structure. The next few paragraphs present spectroscopic x-ray photoelectron spectroscopy results that support this characterization of network disruption and modification.

As noted above, the concentration of network O-atoms contributing to the polarization field associated with the non-bonding pair with 2p π symmetry of the 2-fold coordinated O atoms, and is a linear function of the alloy composition up to a limiting concentration defined as x_λ. In the mean-field approximation, x_λ is obtained by calculating the fraction of O-atoms from the host network SiO_2 that are available to contribute to the polarization field [15]. For Zr silicate alloys, this is estimated to be approximately equal to 0.25 to 0.3, consistent with a saturation of the dielectric constant, k, for as-deposited Zr silicate alloys that has been extrapolated from alloy compositions up to about 20% ZrO_2 [18].

There have been extensive studies of chemical bonding in thin film Zr and Hf silicates that included chemical phase separation (CPS) after high temperature annealing [8,15,16]. The plots in Fig. 3 identify two aspects of these studies. Fig. 3(a) contains a plot of the O 1s binding energy obtained by x-ray photoelectron spectroscopy (XPS) [8] showing a non-linear "s-like" dependence that has been explained in terms of changes in O-atom coordination in different alloy regimes: mixed 2-fold and 3-fold bonding for $0<x<0.5$, and 3-fold and 4-fold bonding for $1>x>0.5$. The "s-like" dependence is correlated with asymmetries in XPS line shapes. A similar plot in Fig. 3(b) is linear when the spectral peak is replaced by a weighted line-shape average binding energy [8]. Fig. 3(c) displays an XPS plot of the Zr $3d_{5/2}$ binding energy versus x. The departure from linearity between x = 0 and approximately 0.25-0.3 is a result of changes in the local bonding of Zr with alloy composition. One contribution comes from the linear increase in coordination of Zr from four to eight in the composition range between SiO_2 and x = 0.5. A second contribution is associated with then network polarization discussed above, and is supported by the model calculations presented in Ref. 8. The value of x_λ~0.25-30 is in agreement with the change in slope of the plot the Zr $3d_{5/2}$ binding energy versus x.

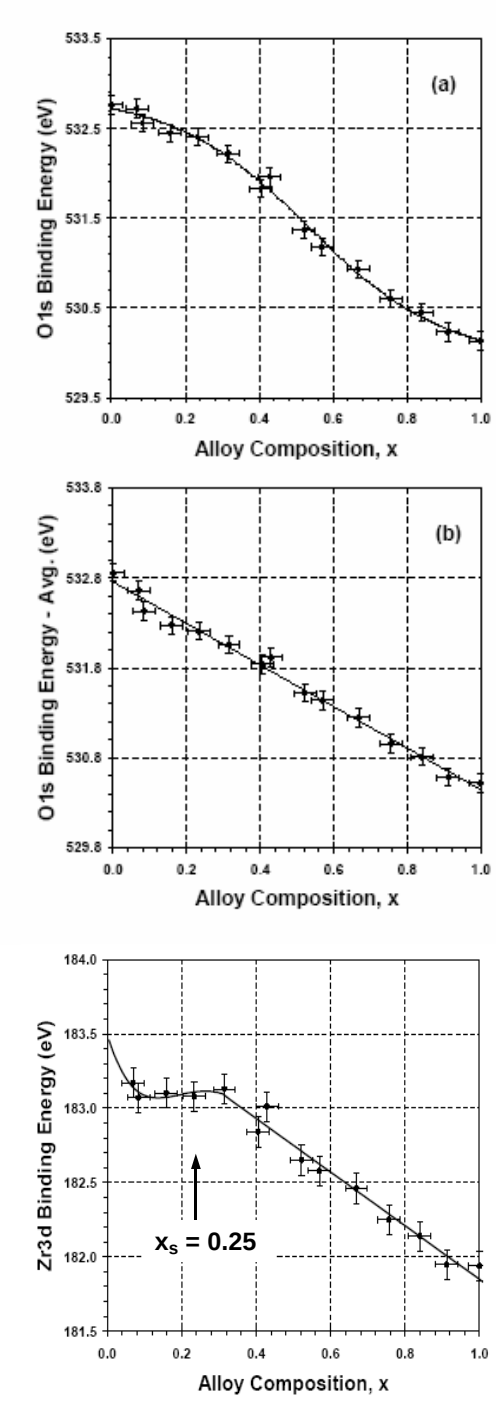

Fig. 3. XPS spectra: (a) O 2s core level, (b) average O 2s core level, (c) Zr $3d_{5/2}$ core level, each vs x.

Other studies by our group have demonstrated that plasma nitridation of Zr and/or Hf silicate films reduces, but does not eliminate chemical phase separation. This has promoted our group to grow pseudo-ternary Zr (and Hf) silicon oxide alloys [6]. These results have identified an *engineering or practical solution* to the high-k dielectric

problem that will carry scaling to 0.7 to 0.8 nm EOT, or equivalently the so-called 35 nm processing node. However, the Si_3N_4 content in these ternary alloys must be controlled within narrow limits to achieve this result.

a-$(SiO_2)_x(Si_3N_4)_y(ZrO_2)_z$ alloys have been deposited at 300°C, and then annealed at temperatures ≥900 °C. Alloys with approximately equal concentrations of SiO_2 and ZrO_2 (40 to 45%), but with smaller concentrations of Si_3N_4, y < 20-25%, display CPS into a-SiO_2 and nanocrystalline ZrO_2 after annealing to 900 °C. This is shown in Figs. 4(a) and (b), which displays detection of CPS by infrared absorption and differentiated x-ray photoelectron spectroscopy (DXPS) studies of the O 1s state binding energy [10]. Alloys with approximately equal concentrations of SiO_2 and ZrO_2, of about 30-35%, and with concentrations of Si_3N_4 between 35 and 40% display spectroscopic evidence for bonding changes for annealing temperatures up to 900 °C (see Figs. 5(a) and (b)). In marked contrast to the alloys with lower Si_3N_4 content, the spectra for the higher Si_3N_4 content alloys do not display features indicating CPS into SiO_2 and ZrO_2 for annealing at temperatures >900 °C. These as-deposited films have mean-field values of $n_c > 3.1$ and $r_c > 3.85$. Network self-organizations occurring for annealing to temperatures greater than 900 °C are discussed in the next section of the paper.

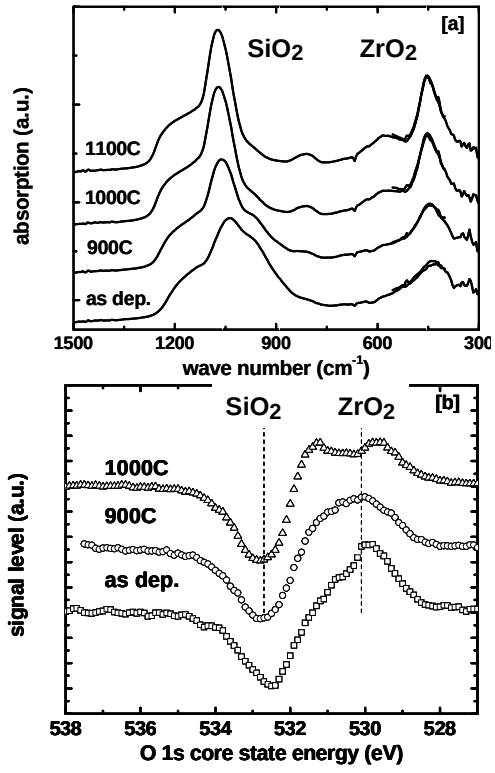

Fig. 4. (a) Infrared and (b) derivative XPS O 1s spectra of a a-Zr Si oxynitride alloy, $(SiO_2)_{0.4}(Si_3N_4)_{0.25}(ZrO_2)_{0.35}$, for as-deposited and annealed thin films.

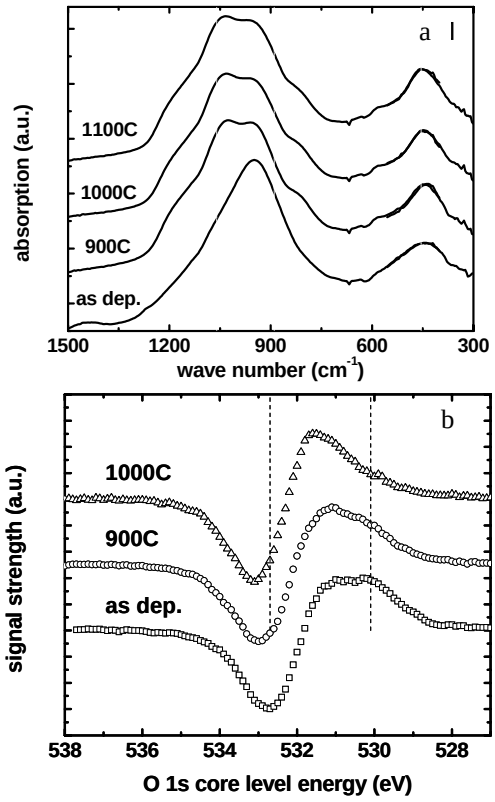

Fig. 5. (a) Infrared and (b) derivative XPS O 1s spectra of alloys with approximately equal concentrations of SiO_2 and ZrO_2 of about 30-35%, and with concentrations of Si_3N_4 between 35 and 40%.

However, it is important to note that the preservation of electron and hole channel mobilities requires a thin interfacial buffer layer of SiO_2 or mono-layer scale nitrided SiO_2 that contributes ~0.3 to 0.35 nm to EOT [14]. This layer is positioned between the c-Si substrate and the a-Zr Si oxynitride dielectric. After annealing to 900 °C in a chemically inert ambient, the Si-O bonding arrangements this thin interfacial buffer layer result from an interfacial strain-relieving network self-organization that has been addressed at length in Ref. 14.

4. Hydrogenated amorphous silicon for TFT and PV applications

Si-atom dangling bond defect concentrations determined by electron spin resonance (ESR) are ~1-2×10^{18} cm^{-3} for optimised a-Si, and reduced to ~5×10^{15} cm^{-3} for hydrogenated a-Si:H with approximately 10 at. % bonded-H [20]. Infrared studies indicate bonded-H is predominantly in monohydride or Si-H arrangements [21]. Optimized films have weaker spectral features associated with a significantly lower concentration of H in dihydride or Si-H_2 arrangements. NMR studies indicate the same two bonding groups: i) a so-called *dilute phase* associated with monohydride (Si-H) groups within small voids (e.g., divancancies), and ii) a *clustered phase* associated with polyhydride (Si-$H_2]_N$) chains [1]. In support of these IR and NMR results, a model for the

transition from SiH to $SiH_2]_N$ bonding, based on plasma and reactive sputtering deposition with controlled surface H availability, yields a universal relationship for the concentration threshold for $SiH_2]_N$ incorporation [22]. These results indicate that ~10% H is the concentration at which incorporation of additional H occurs in $SiH_2]_N$ groups begins. The remainder of this section of the paper addresses and explains these results through an extension of bond-constraint theory [23].

New insights into differences between optimized (i) a-Si, (ii) hydrogenated a-Si:H, and (iii) ternary alloys, e.g., a-Si:H:O, are addressed by extensions of bond-constraint theory to amorphous semiconductors in which the optimization does not necessarily result in good glass formation as in many of the previously research studies, e.g., as in Ge-Se alloys discussed above. This is paramount to understanding that optimization comes in different forms: i) the ideal glass forming properties for the intermediate phase in the Ge-Se alloy system, ii) the minimization of electronically active defects in an a-Si thin films, a iii) an additional reduction in electronically active defects when low concentrations of H are bonded to Si, as in hydrogenated a-Si:H with 5-10 atomic percent hydrogen.

This novel approach to a-Si(H) alloys combines the chemical self-organization mechanism previously identified for intermediate phases [14], with two additional and more recently developed *paradigm* changes: (i) broken bond-bending constraints that derive from asymmetric bonding triads, first addressed in Ref. 24, and (ii) vacancy formation as a pathway to suppressing percolation of localized bond-strain. The concept of vacancy formation builds on a chemical self-organization first identified in spectroscopic studies of hydrogenated Si_3N_4 [25]; and more recently in Zr and Ti Si oxynitride ternary alloys, and chemically phase separated inverted silicates, such as $(HfO_2)_{0.8}(SiO_2)_{0.2}$ [15,16,17,26].

The application of BCT, including broken constraints, and self-organizations for suppression of strain percolation, is first applied to a-Si. If each 4-fold coordinated Si atom were incorporated into a completely connected and disordered network, and C_{av} would include 5 bond-bending + 2 bond-stretching constraints per atom, and be equal to 7 constraints/atom; this is more than a factor of 2 higher than for an ideal, or defect free network solid. By comparison, *non-hydrogenated* Si_3N_4 with N_{av} = 3.4 and C_{av} ~ 4.4 constraints/atom, is a highly defective insulator, with more than $5x10^{18}$ defects-cm^{-3}. The defect density in Si_3N_4 is reduced significantly by introducing more 20-30 at. % hydrogen that is incorporated in *hydrogen bond-coupled* N-H groups that reside in internal voids or cavities. This localized clustering of H is shown schematically in Fig. 6(a). These high levels of H-atom reduce defect densities below 10^{17} cm^{-3}, or equivalently 5×10^{11} cm^{-2}. As noted above in Section 2, this makes hydrogenated Si_3N_4 the dielectric of choice for TFTs, the switching elements in liquid crystal displays, LCDs, for laptop computers and flat panel television monitors.

This insight into the low defect density in hydrogenated Si nitride has stimulated us to propose a similar defect reduction mechanism for a-Si:H. This development has evolved in two steps, each driven by two experimental results: i) the electron spin density is ~10^{18} cm^{-2} in optimized a-Si that has density deficiency of about 5%, and ii) the lowest defect density in a-Si;H which occurs for a bonded H concentration of ~10% and corresponds to a concentration that marks the threshold for detection by IR of dihydride, $Si\text{-}H_2$, bonding in addition to Si-H [21,22].

The experimental determined density deficit of 5-7%, is equates to a divacancy density of approximate 2×10^{20} cm^{-3}. These divacancies contain 6 dangling bonds associated with removal of 2 Si atoms; four of these can reconstruct into 2 strained bonds as in crystalline Si [27], or alternatively remove spins by self organizing into pairs of Si atoms: One member of the pair has an unoccupied terminal bond, here designated as Si^+, and the member of the pair is doubly occupied, here designated as Si^-. In this notation, the ESR active Si dangling bond with one electron is designated as Si^o. This optimization relationship is given by

$$2\ Si^o \rightarrow Si^+ + Si^-, \qquad (1)$$

and is known to be a negative U reaction, where the electron repulsion in the S member is more than compensated by a local relaxation in which there is a distortion of the tetrahedral bonding geometry of the Si atom. The reaction in Eqn. (1) also occurs in on the Si(111) surface, as for example in the 7x7 surface reconstruction [28].

Returning now the BCT, and addressing the net spin density from a more general perspective of constraint counting. Si atoms on divacancy internal surface are bonded 18 nearest-neighbors Si atoms that encapsulate the void space of the divacancy. Each of these 18 Si atoms can have broken bond-stretching and bond-bending constraints in addition to those associated with the 6 terminal atoms of the divacancy internal surface.

The broken constraints *amplify* the effect of the divacancy inclusions on network strain reduction, and are in place for ~25% of the network Si atoms. If we now assume asymmetric tetrahedral arrangements on 25% of the Si atoms, this effects primarily the bond-bending constraints, and reduces the number of these constraints/atoms to ~2.33 rather than 5. In addition the number of stretching constraints of a third of these atoms are reduced as well due to the removal of 2 Si-atoms that creates the vacancy. This brings the effective number of constraints for 25% of the Si atoms to approximately 4. The average number of constraints/Si atom with the ~ 5 % density is then given by $C_{av} = 0.75\times7 + 0.25\times4 = 6.25$, which in turn corresponds to N_{av} = (6.25+3)/2.5 or 3.7 [23]. N_{av} is then 1.3 more than the *value* of 2.4 for an ideal and essentially *defect free* network. Based on an empirical scaling relationship between over-coordination, $N_{av} > 2.4$, and the resulting defect concentration [29], this effective over-coordination of 3.7 corresponds to a defect density of ~1.5×10^{18} cm^{-2}, approximately the same the lowest density of spins reported for a-Si prepared by magnetron sputtering at a substrate temperature of ~300 K [20]. This

defect density is also approximately equal to the *intrinsic* density of dangling bonds at Si-SiO_2 interfaces where the interfacial step between N_{av} for SiO_2 (2.67) and the c-Si substrate (4) is also 1.3.

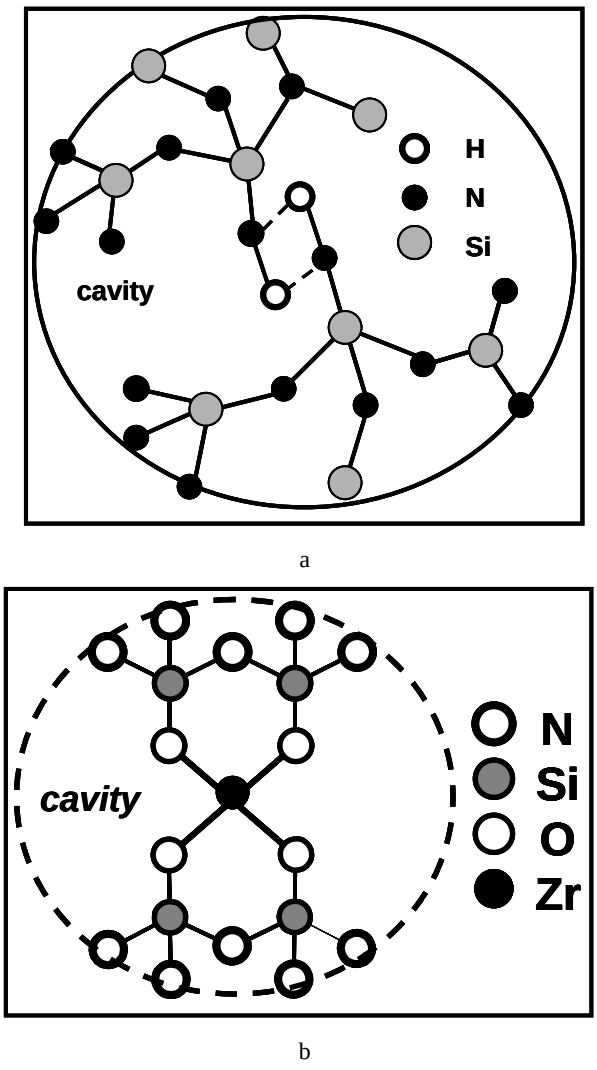

Fig. 6. (a) Schematic representation of the H-bonding interaction between H-terminated N-atom dangling bonds embedded in localized cavities in a Si-N matrix as in $Si_{0.30}N_{0.40}H_{0.30}$. (b) Schematic representation of the local bonding environments of Zr-, Si-, O- and N-atoms in a Zr Si oxynitride alloy with ~40% Si_3N_4, and equal SiO_2 and ZrO_2 concentrations of ~30%.

The addition of ~10% H to a-Si is well-known to reduce the defect density, the number of neutral Si^o dangling bonds determined by ESR, in a-Si:H to between $5x10^{15}$ to 10^{16} cm^{-3}, or by a factor of ~150 to 300. Hydrogenation of the Si-SiO_2 interface by annealing in a forming gas mixture of H_2 and H_2 at ~400-450°C reduces the density of interfacial traps to approximately $1\text{-}2x10^{10}$ cm^{-2}, also by a factor of 100 to 200. There is then a close quantitative similarity between the effectiveness of H-passivation of dangling bond defects at Si-SiO_2 interfaces, and in dangling bond termination of defects in a-Si:H. It is equally interesting that defects are not as effectively terminated in a-Si i) by reduced levels of H-incorporation in the range of 3 to 5 % H as the substrate temperature is increased above 300 °C for plasma CVD depositions, and ii) by increased levels of H-incorporation in excess of 20% and in $SiH_2]_N$ local bonding (in the so-called *clustered phase* []), as the substrate temperature for deposition is reduced below 200 °C for the same class of plasma CVD depositions. Fig. 7 is schematic representation of this defect behavior that treats the optimized or lowest dangling bond density material as an intermediate phase, that is bracketed between stress-rigid and floppy regimes, for lower and higher H-atom content, respectively. Fig. 1(a) displays a qualitatively and quantitatively similar behavior of defect densities in hydrogenated Si-N alloys. In this case the defect density is tracked by the channel mobility of a TFT device. The current in regimes designated as stressed-rigid and floppy, respectfully, is reduced due to interfacial trapping in the dielectric during channel current flow; hence a reduced, or trapped-controlled drift mobility.

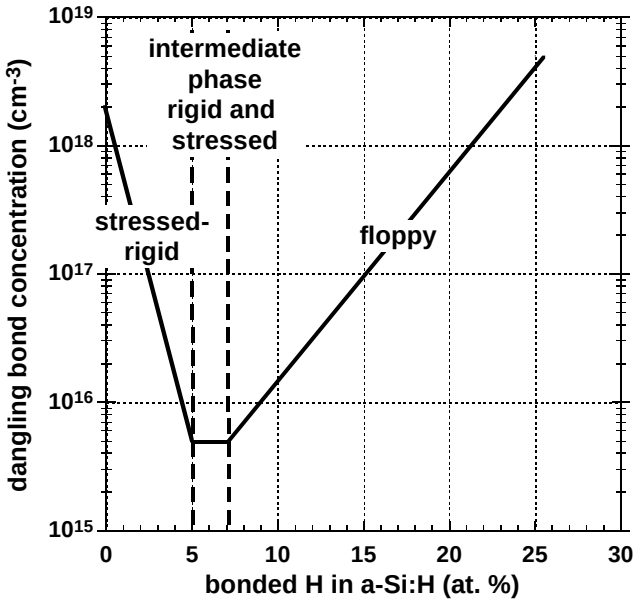

Fig. 7. Schematic representation of the relative dangling bond defect density in hydrogenated amorphous silicon, a-Si:H. This includes three different alloys regimes, in order of increasing H-content: i) a floppy phase, ii) a stressed and rigid intermediate phase, and iii) a stressed-rigid phase in which bond – stress has percolated throughout the sample.

In a paper presented a recent conference [12], one of the authors, JCP, noted that "many physical systems are not crystalline, yet they exhibit remarkable properties as a result of optimization", and that "examples include: network glasses (added for emphasis, discussed by Boolchand et al., [14]), including window glass; organic glasses, such as glycerol; the Si/SiO_2 interface", (added for emphasis, where symmetry broken constraints were first applied [24]).

This section of the paper has presented a very important application of this universal and elegant concept by the application to a technologically important material, a-Si:H. There are other non-crystalline technologically important alloy systems, the pseudo-ternary alloys of groups IVB transition metal oxides, such as TiO_2, ZrO_2 and HfO_2, along with SiO_2 and Si_3N_4 that display qualitatively similar, defect reducing self-organizations that make them ideal candidates for future generations of advanced Si and compound semiconductor (SiC and GaAs) [26]. Spectroscopic studies indicate that in these materials, as well a-Si(H) and hydrogenated Si nitride discussed in Section 3, that include strain-reducing self-organizations that occur in a limited regime of compositions, and that these self-organizations are the pathway to *optimization* in the context of minimizing electronically-active defects.

In each of the examples discussed above, a-Si, a-Si:H, a-Si_3N_4, and the Ti/Zr/Hf high Si_3N_4 Si oxnitride alloys, the constituent atoms self-organize into nano-scale clusters with non-statistical or chemically ordered bonding arrangement. These self-organizations prevent percolation of macroscopic strain, and result in mean-field C_{av} values that optimize defect concentrations for the respective bonding chemistries.

Measurements on a-Si:H:O alloys [31,32], and a-Si:H:N [335] indicate non-statistical bonding arrangements, e.g., O and H atoms bonded to the same Si atom in a-Si:H:O alloys. These arrangements are also typical of intermediate alloy phases that result in decreases in defects and defect precursors. As shown in Refs 31 and 32, the addition of O to a-Si:H in a narrow range of compositions improves luminescence and photoconductivity, reinforcing relationships between optimization and device applications.

5. Summary

In summary, this paper has applied the concepts of network self-organizations with increased in chemical-ordering, broken bond bending constraints to several important non-crystalline alloy systems. The commonality among these alloy systems, is that the self-organizations and accompanying intermediate phases have been enabling for important device applications. These results are now summarized below.

The composition, $Si_{0.3}N_{0.4}H_{0.3}$, has $N_{av} = 2.7\pm0.05$, and $C_{AV} = 3.05\pm0.1$, has been addressed in Section 3. These values of N_{av} and C_{av} are indicators of a network self-organization that suppresses percolation of network rigidity, thereby reducing defects that trap channel electrons during TFT operation. In this intermediate phase regime, Si-N bonds form a rigid, but strain free network backbone that encapsulates Si-N-H bonding groups, and thereby suppresses the percolation of network rigidity. This example represents the first *device performance detection* of an intermediate phase. The general reader is referred to a recent publication, Ref. 19, which provides a broader view of how the work reported in this paper relates to basic of aspects of rigidity as applied in the glass science community and literature.

As addressed in Section 4, similar chemical ordering self-organizations also occur in a-$(SiO_2)_x(Si_3N_4)_y(ZrO_2)_z$ alloys deposited at 300 °C and processed at higher temperatures ≥900 °C. Alloys with x and z approximately equal to 0.3 and with a higher concentration of Si_3N_4, y > 0.3, display spectroscopic evidence for bonding changes for annealing temperatures up to 900 °C, but the absence of CPS for annealing at temperatures >900 °C. As-deposited films have mean-field values of $N_{av} = 3.1$ and $C_{AV} = 3.85$. After 900 °C annealing, IR and XPS spectra for these alloys are consistent with a network self-organization with non-crystalline Zr silicate groups *encapsulated in a cavity inside of a* rigid, but strain-free Si_3N_4 *backbone*. This structure has r_c and n_c values given by: $N_{av} = 2.77\pm0.07$ and $C_{av} = 3.2\pm0.1$. The values of C_{av} are about the same as those, $C_{av} = 3.0$ to 3.3, of glasses and thin films in the intermediate phase regime of Ge_xSe_{1-x} alloys.

Qualitatively similar bonding of terminal O-atoms in a-$(SiO_2)_x(Si_3N_4)_y(ZrO_2)_z$ alloys, and terminal SiN-H and Si-H groups in a-$Si_xN_yH_{1-x-y}$ alloys, are responsible for the low values of n_c; i.e., the Si-N-H bonds are also directed into a *cavity* inside a rigid, but strain free Si_3N_4 *backbone*. These result from *functionally equivalent* chemical self-organizations that prevent percolation of network stress, thereby avoiding formation of point defects, and/or CPS that would degrade TFT and FET performance. Figs. 6(a) and 6(b) indicate schematic representations of these bonding arrangements. Qualitatively similar self-organizations are enabling for the integration of optimized a-Si(H) thin films in both TFTs and PV devices, as addressed in detail in Section 5. In this alloy system, the prevention of strain percolation and the accompanying defect reductions are accomplished by a chemical self-organization that introduces small voids; in our model calculation these are divacancies. Although the details are different, the chemical self-organizations in the a-$(SiO_2)_x(Si_3N_4)_y(ZrO_2)_z$ alloys, the in a-$Si_xN_yH_{1-x-y}$ alloys, and a-Si:H and a-Si:H:O(N) are qualitatively similar to each other, but rather different than in the Ge-Se alloys.

In summary, the commonality in for all four alloy systems addressed immediately above is embodied in i) chemical bonding self-organizations which increase chemical order at the expense of reductions in configuration entropy, but have a more than compensating effect on the reduction of bond-strain energy, ii) the breaking of bond-bending constraints associated directly with increases in chemical ordering, iii) formation of intermediate phases over narrow composition ranges, iii) reductions in defects and defect precursors which are property of these intermediate phases.

6. Epilogue

Many of the research results of this paper, particularly those related to a-Si, were derived in large part from the intellectual stimulation created of the seminal papers authored by Professor Radu Grigorovici and his

co-workers in the 1960's. The mostly widely quoted among these was a paper co--authored with J. Tauc and A. Vancu, published in 1966, and titled "Optical Properties and Electronic Structure of Amorphous Germanium" [33]. This paper has received 892 citations to date. This paper was proceeded by a paper by Grigorovici et al, published in 1965, and titled "Electrical Properties of Evaporated Si and Ge layers" [34]. Four other papers, [35-38], dealing with the properties and structure of amorphous Si and Ge were also published between 1966 and 1968, the most cited of these [37], "Amorphous Germanium and Silicon: Structure and Transport Phenomena", received 54 citations. Thank you again Professor Grigorovici for pointing the way, and stimulated the interest in these two important amorphous materials. These studies brought a-Si and a-Ge into the rapidly develop field of amorphous semiconductors, being cited more than 1000 times, leading eventually to the discovery of doping in a-Si(H), and finally the integration of a-Si(H) and doped a-Si(H) into photovoltaic and thin film transistor devices.

Acknowledgements

This research is supported by the Office of Naval Research, ONR, and the Semiconductor Research Corporation.

References

[1] G. N. Parsons, C. Kusano, G. Lucovsky, J. Vac. Sci. Technol. **A 5**, 1655 (1987).
[2] S. S. Kim, G. N. Parsons, G. G. Fountainm, G. Lucovsky, J. Non-Cryst. Solids, **115**, 69 (1989).
[3] G. Lucovsky, S. S. He, M. J. Williams, D. Stephens, Microelectron. Eng. **25**, 329 (1994).
[4] G. D. Wilk, R. W. Wallace, J. M Anthony, J. Appl. Phys. **87**, 484 (2000); J. Appl. Phys. **89**, 5243 (2001).
[5] C. Krug, G. Lucovsky, J. Vac. Sci. Technol. **A 22**, 1301 (2004).
[6] P. Boolchand, X. Feng, W. J. Bresser, J. Non-Cryst. Solids **293**, 348 (2001).
[7] G. Lucovsky, IBM J. of Res. and Dev. **43**, 301 (1999).
[8] G. B. Rayner, D. Kang, Y. Zhang, J. L. Whitten, G. Lucovsky, J. Vac. Sci. Technol. **B 20**, 1748 (2002).
[9] G. Lucovsky, J. C. Phillips, J. Non-Cryst. Solids **266**, 1335 (2000).
[10] B. Ju, Ph. D. Dissertation, Department of Materials Science and Engineering, May 2005.
[11] P. Boolchand, D. G.Georgiev, B. Goodman, J. Optoelectron. Adv. Mater. **3**, 703 (2001).
[12] K. Xiong, J. Robertson, Microelectron. Eng. **80**, 408 (2005).
[13] G. Lucovsky, et al., Microelectron. Eng. **80**, 110 (2005).
[14] G. Lucovsky, J. C. Phillips, J. Vac. Sci. Technol. **B 22**, 2089 (2004); G. Lucovsky, J. P. Maria, J. C. Phillips, J. Vac. Sci. Technol. **B 22**, 2099 (2004).
[15] G. B. Rayner, D. Kang, G. Lucovsky, J. Vac. Sci. Technol. **B 21**, 1783 (2003).
[16] G. B. Rayner, D. Kang, G. Lucovsky, J. Non-Cryst. Solids **338**, 151 (2003).
[17] J. P Maria, D. Wichakana, J. Parrete, A. I. Kingon, J. Mater. Res. **17**, 1571 (2002).
[18] G. Lucovsky, R. B. Rayner, Appl. Phys. Lett. **77**, 2912 (2000).
[19] P. Boolchand, G. Lucovsky, J. C. Phillips, M. F. Thorpe, Phil. Mag. **85**, 3823 (2005).
[20] J. A. Reimer, R. W. Vaughan, J. C. Knights, Solid State Commun. **37**, 161 (1981).
[21] G. Lucovsky, R. J. Nemanich, J. C. Knights, Phys. Rev. **B 19**, 2064 (1979).
[22] G. Lucovsky, G. N. Parsons, C. Wang, B. N. Davidson, D. V. Tsu, Solar Cells **20**, 121 (1989).
[23] J. C. Phillips, J. Non-Cryst. Solids **34**, 153 (1979); **43**, 37 (1981).
[24] G. Lucovsky, J. C. Phillips, Appl. Phys. A: Mater. Sci. Process **78,** 453 (2004).
[25] G. Lucovsky, J. C. Phillips, J. of Physics-Condensed Matter **16**, S5139 (2004).
[26] G. D. Watkins, J. W. Corbett, R. M. Walker, J. Appl. Phys. **30**, 1198 (1959).
[27] D. J. Chadi et al., Phys. Rev. Lett. **44**, 799 (1980).
[28] G. Lucovsky, Y. Wu, H. Niimi, V. Misra, J. C. Phillips, Appl. Phys. Lett. **74**, 2005 (1999).
[29] J. C. Phillips, at From Solid State to BioPhysics III, Dubrovnik, Croatia, 24 June to 1 July 2006.
[30] M. A. Paesler, D. A. Anderson, E. C. Freeman, G. Modde, W. Paul, Phys. Rev. Lett. **41** 1462 (1978).
[31] J. C. Knights, R. A. Street, G. Lucovsky, J. Non-Cryst. Solids **35-36**, 279 (1980).
[32] M. D. Williams, S. S. He, S. M. Cho, G. Lucovsky, J. Vac. Sci. Technol. **A12**, 1072 (1994).
[33] J. Tauc, R. Grigorovici, A Vancu, Physica Status Solidi **15**, 627 (1966).
[34] R. Grigorovici, et al., Revue Roumaine de Physique **10**, 649 (1965).
[35] R. Grigorovici, N. Croitoru, A. Devenyi, Physica Status Solidi **16**, K143 (1966).
[36] R. Grigorovici, N. Croitoru, A. Devenyi, Physica Status Solidi **23**, 627 (1967).
[37] R. Grogorovici, Materials Research Bulletin **3**, 13 (1968).
[38] R. Grigorovici, A. Vancu, Thin Solid Films **2**, 105 (1968).

*Corresponding author: glucovsky@aol.com